ISPRS Annals of the Photogrammetry, Remote Sensing and Spatial Information Sciences, Volume X-5/W4-2025
Philippine Geomatics Symposium (PhilGEOS) 2025 "Enhancing Human Quality of Life through Geospatial Technologies",
24–25 November 2025, Quezon City, Philippines

Modeling urban expansion in the Philippines using a cellular automata–integrated spatiotemporal machine learning framework

Joshua R. Dela Cruz[1], Adrian Roy L. Valdez[2]

[1]Artificial Intelligence Program, University of the Philippines Diliman - delacruz.joshua.reyes@gmail.com
[2]Scientific Computing Laboratory, University of the Philippines Diliman - alvaldez@up.edu.ph

Keywords: Urbanization, Spatiotemporal modeling, Cellular Automata, Long Short-Term Memory (LSTM), Machine learning, Geospatial data

Abstract

Urbanization in the Philippines rapidly shift towards a certain critical level, yet there are only few established frameworks that provide localized forecasts of urban growth across the Philippines, making it difficult to identify which specific cities are likely to thrive or be left behind, a gap that poses significant challenges for effective urban planning. This study introduces a spatiotemporal modeling framework that combines Long Short-Term Memory (LSTM) networks with Cellular Automata (CA) to simulate urban expansion at a national scale. Using open-source geospatial data on land use, slope, transportation, and urban footprints, the model generates dynamic urban transition probabilities through LSTM, which are then fed into a CA system that simulates urban sprawl. After simulation, the comparison of the generated maps with the actual maps showed that hybrid approach outperformed conventional methods such as standalone LSTM, and traditional Logistic-Regression CA, achieving a Fuzzy Similarity Rating (FSR) of 38.20% and a figure of merit (FOM) of 55.37%, highlighting emerging urban hotspots such as Calamba, Carcar City, and Davao City by 2030. The integrated LSTM-CA model captures spatial interactions and temporal dynamics more effectively than static models, offering improved realism in simulating pixel-level transitions. By offering data-driven forecasts of urban growth, this study supports a more informed spatial planning decisions, including infrastructure development and land conservation. With more sustainable and inclusive urbanization, this aims to ensure that no city is left behind as the country moves toward its urban future.

1. Introduction

By 2050, an estimated 84% of Filipinos are projected to reside in urban areas UN-Habitat (2023), a significant increase from just 54% in 2020 census Philippine Statistics Authority (PSA) (2022). In less than three decades, the Philippines is expected to experience a level of urban transformation that historically occurred over centuries.

When well-planned and managed, urbanization can serve as a powerful engine for economic growth, offering opportunities for poverty reduction and improved quality of life. However, despite its expanding economy, the Philippines has largely failed to harness the full benefits of urbanization. Unplanned urban growth has resulted in overcrowded neighborhoods, traffic congestion, fragmented policy implementation, and increasing vulnerability to climate-related risks Chaves et al. (2022). Without strategic intervention, the country risks facing an unsustainable urban future.

Despite the scale and urgency of the issue, there remains a scarcity of studies offering localized, data-driven projections of urban growth across the Philippine archipelago to understand the behavior of urban growth and identify which cities will be specifically affected by it. One of the few nationwide attempts at modeling urban expansion was focused primarily on estimating future flood hazards, rather than addressing urban growth dynamics directly Johnson et al. (2021).

Most existing forecasting efforts are limited in scope, typically concentrating on individual regions or metropolitan centers Estoque and Murayama (2012). Although the results of these subnational scale studies provide useful information for local planning processes, they largely overlook the broader spatial and temporal dynamics necessary for understanding and managing nationwide urban expansion necessary to support central government agencies.

This research seeks to address this critical gap by integrating machine learning techniques with the widely adopted Cellular Automata (CA) modeling approach with the goal of enhancing both the accuracy and adaptability of urban growth simulations. Specifically, the study proposes a framework capable of generating spatially explicit forecasts of urban expansion across the entire Philippine archipelago. By doing so, it enables the production of localized predictions that identify where urban growth is most likely to occur, essential for helping cities expand more intelligently and sustainably.

2. Related Works

2.1 Cellular Automata for Forecasting Urban Expansion

Despite the inherent complexity of urban systems White and Engelen (1993), CA has become one of the most widely adopted modeling frameworks for simulating urban growth due to its simplicity and flexibility. Urban CA models operate on the principle that the evolution of land use is influenced by the current and neighboring land-use states, aligning well with the idea that historical patterns of development significantly influence future expansion. As computing capabilities have advanced, CA models have evolved to incorporate a broader set of spatial and temporal data, allowing for more sophisticated representations of urban dynamics Santé et al. (2010).

A conventional urban CA model typically comprises four core components: (1) transition rules, which determine how cells change state; (2) neighborhood configuration, which defines the spatial influence of adjacent cells; (3) simulation time steps; and (4) stochastic perturbations to introduce randomness Yeh

This contribution has been peer-reviewed. The double-blind peer-review was conducted on the basis of the full paper.
https://doi.org/10.5194/isprs-annals-X-5-W4-2025-213-2026

and Li (2006). Notable work in this field demonstrated the robustness of CA models through sensitivity analyses of these key components. The study calibrated various transition rule generators including logistic regression, decision trees, and ensemble models, and evaluated the impact of different neighborhood sizes and stochastic parameters. Their tuned model achieved considerable good results on spatial metrics such as PAFRAC, NLSI, CLUMPY, and Aggregation Index, highlighting the capacity of CA to model complex urban phenomena Li et al. (2014).

Further advancements were made through the incorporation of temporal contextual information into CA models. A recent study introduced the Logistic Trend-CA model, which leverages historical urban sprawl trends to enhance long-term forecasting accuracy. The model achieved improvement in predictive performance, as measured by the Figure of Merit (FoM), over traditional CA approaches Li et al. (2020).

2.2 Integrating Machine Learning with Cellular Automata

Several recent works have enhanced the transition rule component of CA by incorporating classical machine learning algorithms to enable more data-driven estimation of urban change suitability through analysis of a wide range of input features. In a study that conducted a detailed calibration process using different combinations of hyperparameters, ML algorithm variants such as Random Forest (RF) and Support Vector Machines (SVM), sample sizes, and zoning configurations to simulate urban sprawl from 2000 to 2030, simultaneous consideration of various spatial determinants of urban growth setup enabled the creation of more accurate transition probability maps, although these maps were generated statically only for each simulation. The study found that RF- and SVM-driven CA models achieved superior performance when trained on larger sample sizes, validating the potential of ML-enhanced transition functions for sprawl modeling Rienow et al. (2021).

Despite these improvements, limitations remain in such frameworks, particularly when applied at the national scale. One key shortcoming lies in the use of static transition probability surfaces, which fail to account for the temporal evolution of spatial patterns. To address this, a more recent study proposed a temporally dynamic CA-ML model incorporating a rich set of 36 features, including time-lagged and spatial-lagged variables Kim et al. (2022). This study leveraged Random Forests, Artificial Neural Networks (ANN), and Extreme Gradient Boosting (XGBoost) to capture both spatial and temporal dependencies more effectively.

The inclusion of multivariate spatial-temporal features significantly improved predictive accuracy across multiple models, thereby demonstrating the value of deeper feature engineering in CA-ML frameworks. These advancements serve as critical foundations and points of inspiration for the framework proposed in this study, which seeks to produce reliable, spatially explicit urban expansion forecasts at a national scale.

3. Methodology

Figure 1 illustrates the overall workflow of the study. It shows the dataset used, their sources, and how they were preprocessed. This also presents how the machine learning model was trained and tested, and finally how the resulting outputs were integrated into the cellular automata for simulation. The following subsections describe each step in detail.

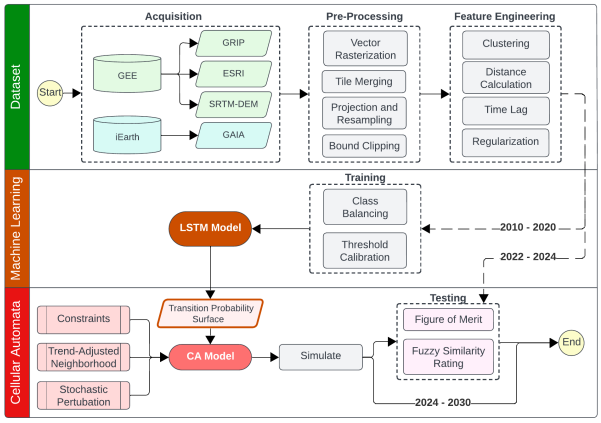

Figure 1. Overall workflow of the study methodology.

3.1 Study Area

The region of interest in this study is the entire Philippines, officially the Republic of the Philippines. It is an archipelagic country in Southeast Asia located in the western Pacific Ocean, comprising 7,641 islands that stretches about 1,150 miles (1,850 km) from north to south, with an east-west span of up to 700 miles (1,130 km) at its widest point in the south. It has a total land area of approximately 300,000 square kilometers. These islands are grouped into three major geographical divisions: Luzon (north), Visayas (central), and Mindanao (south).

The country's archipelagic nature results in a highly fragmented spatial structure, characterized by regional disparities in geography, infrastructure, and development. Major urban centers such as Metro Manila in Luzon, Cebu City in the Visayas, and Davao City in Mindanao are geographically isolated from one another, yet remain interconnected through national-level policies and economic activities such as trade and transportation.

Given these spatial complexities, modeling urban growth across the entire nation using a unified configuration presents both a challenge and an opportunity. By applying a consistent set of features and modeling parameters across all regions, this study aims to capture the diverse urban dynamics at both local and national scales. Such an approach is intended to yield more coherent and comprehensive urban growth forecasts that can inform nationwide spatial planning and policy development.

3.2 Data

This study utilizes four primary datasets, summarized in Table 1 and illustrated in Figures 2 to 5. Figures 4 and 5 additionally present derived feature maps, which are further discussed in Section 3.2.2.

3.2.1 Acquisition and Pre-processing: The GRIP, ESRI, and SRTM datasets were accessed via Google Earth Engine (GEE) provided by the community-contributed dataset catalog Roy et al. (2025). Clipping to the Philippine boundary was the first basic preprocessing done to reduce memory and storage requirements, as the original datasets are global in scope. Meanwhile, the GAIA dataset was obtained from the *iEarth Datahub* Observatory, which provides downloadable tiled raster data. Unlike GEE, which requires some familiarity with JavaScript for querying and preprocessing, iEarth offers a user-friendly interface for selecting and downloading data tiles. However,

This contribution has been peer-reviewed. The double-blind peer-review was conducted on the basis of the full paper.
https://doi.org/10.5194/isprs-annals-X-5-W4-2025-213-2026 | © Author(s) 2026. CC BY 4.0 License.

Name	Description	Usage	Feature Type	Reference
Global Roads Inventory Project (GRIP) v4	Vector dataset of global roads including highways, primary, and local roads	Used to compute distance to nearest road	Static	Meijer et al. (2018)
ESRI 10m Annual Land Cover	Global land use/land cover classification with 9 classes, produced by Impact Observatory	Used to extract location of water	Static	Karra et al. (2021)
Shuttle Radar Topography Mission (SRTM) v4.1	Global digital elevation model from NASA	Used as slope input features	Static	Reuter et al. (2007)
Global Artificial Impervious Areas (GAIA), v2024	Annual global urban extent mapping (urban vs. non-urban)	Used as the dependent variable, and to derive distance to urban areas and urban clusters	Dynamic (2010–2024)	Gong et al. (2020)

Table 1. Summary of datasets used in the study

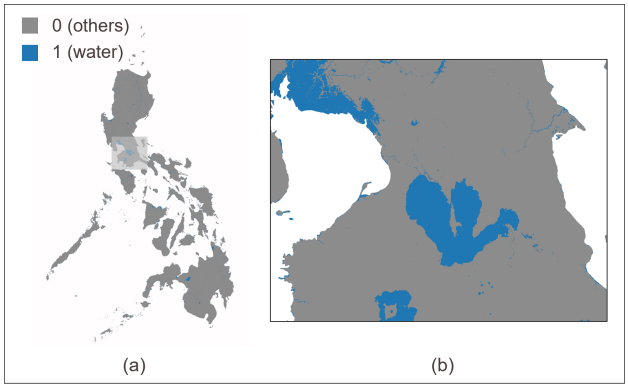

Figure 2. Visualization of ESRI water land classification data: (a) nationwide map of the Philippines, and (b) zoomed-in view.

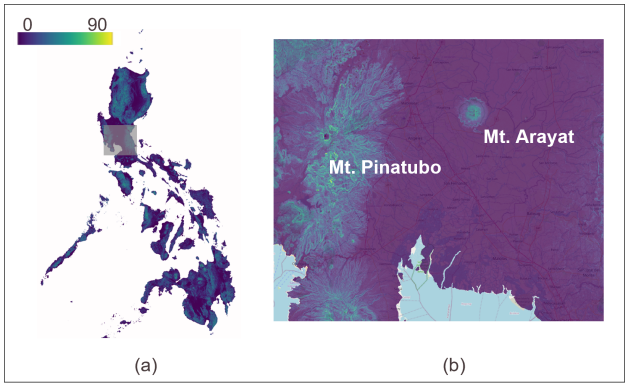

Figure 3. Visualization of SRTM slope data: (a) nationwide map of the Philippines, and (b) zoomed-in view.

the process of downloading specific annual layers must be done manually per year. All datasets were then pre-processed using the `rasterio` Python library, allowing for automated processing across multiple files. The pre-processing pipeline included the following steps:

- The GRIP dataset, originally in vector format, was rasterized. Each pixel intersected by a road segment was assigned a value of 1.
- The ESRI land cover dataset contained nine land use classes; only the class corresponding to water bodies was extracted and saved as a binary raster mask.
- GAIA, which was downloaded as multiple raster tiles, was mosaicked into a single image for each year. An additional step called pixel correction Gómez et al. (2020) was applied to enforce temporal consistency: once a pixel was classified as urban in a given year, it remained urban in all subsequent years. This reflects the assumption that urban areas do not revert to non-urban over time.
- All raster files were reprojected from their original coordinate system (CRS EPSG:4326) to UTM Zone 51N (EPSG:32651), which is appropriate for the Philippine region. This conversion allowed for all spatial units to be in meters.
- All images were resampled to a common spatial resolution of 100 m $\times$ 100 m, selected based on the coarsest resolution among the datasets and to reduce the overall memory requirement during processing.
- Finally, the rasters were clipped again using a more detailed national boundary of the Philippines Faeldon (2024). All areas outside this boundary including surrounding water bodies were assigned a designated `noData` value.

3.2.2 Feature Engineering: To extract relevant spatial characteristics from the raw datasets and enhance the dynamic modeling capabilities of machine learning model in generating the transition probability surface, the following feature engineering procedures were performed:

- Studies on diffusion models though often focusing on population spread, suggest that in densely populated regions, where centroids are close together, urban expansion typically occurs over shorter distances from the center. In contrast, in rural areas where urban clusters are more dispersed, expansion tends to occur across broader distances Wu and Martin (2002). This is intuitive: in densely built-up regions such as Metro Manila, most land near the centroid is already urbanized, so new development is likely to emerge only at a certain distance away from the centroid. Conversely, in rural regions where the centroid of small clusters is located far from these clusters, urban development tends to emerge far from the centroid and near these more isolated clusters.

  Clustering of urban areas was implemented using the `k-means` algorithm from the cuML Python library, utilizing default initialization parameters.

  To determine the optimal number of clusters k, a grid search was conducted for each regional urban map (Luzon, Visayas, Mindanao) per year, using silhouette score as the selection criterion. The optimal k was then fixed and used throughout the simulation. The silhouette score evaluates the cohesion and separation of the resulting clusters and is especially effective when ground-truth labels are unavail-

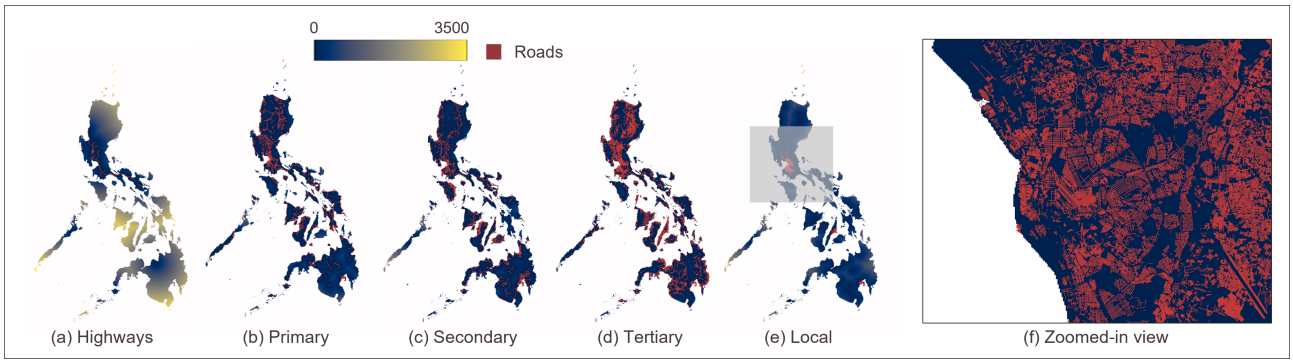

Figure 4. Visualization of nationwide distance maps from the GRIP dataset for different road classification: (a) highways, (b) primary roads, (c) secondary roads, (d) tertiary roads, and (e) local roads; (f) zoomed-in view of local road distance.

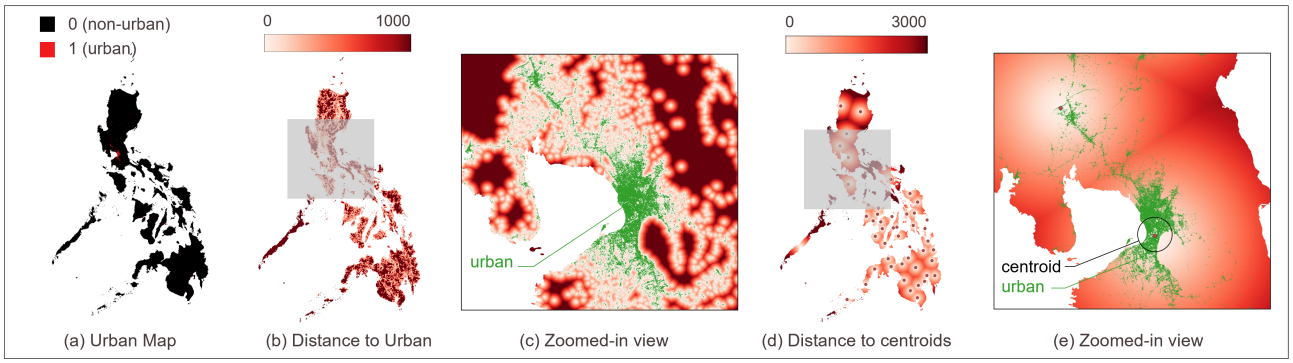

Figure 5. Visualization of nationwide maps from the GAIA dataset: (a) urban extent, (b) distance to urban areas, (c) zoomed-in view of distance to urban areas, (d) distance to urban cluster centroids, and (e) zoomed-in view of distance to urban cluster centroids.

able, as in this study. Higher silhouette scores indicate better-defined clusters Rousseeuw (1987).

- Using the rasterized road maps and the urban centroids, new feature maps were generated by calculating the Euclidean distance of each pixel to the nearest target pixel. To handle the large memory size of the dataset efficiently, this was implemented using a parallelized method.

  The operation was implemented using RAPIDS cuCIM's morphology function `distance_transform_edt`, which calculates the shortest distance from each foreground (non-zero) pixel to the nearest background (zero) pixel. The approach uses parallel banding for computational efficiency Cao et al. (2010).

- Time lag is a common temporal variable used in autoregressive models, based on the idea that the current value of a time series can be approximated as a linear combination of its past values plus some random noise. Previous studies have shown that spatio-temporal lags are crucial in capturing the variability of urban expansion and are easily integrable into land-use change models Kim et al. (2022).

  However, unlike conventional time series models dealing with continuous values, this study focuses on binary classification. Hence, no autocorrelation studies were conducted to determine the optimal number of lag years. Instead, a simple lag-1 approach was adopted: the urban footprint map at time t is used as an input for predicting the state at time $t + 1$, and so on.

- After generating and finalizing all feature maps with metadata presented in Table 2, standardization was applied to ensure that features with different units and scales do not disproportionately influence the model. Standardization rescales features to have a mean of 0 and a standard deviation of 1. This was implemented using RAPIDS cuML's `StandardScaler` module.

Parameter	Value
CRS	EPSG: 32651
Bounds	left = -221000, bottom = 504000, right = 927700, top = 2355900
Resolution	100m × 100m
Shape	11,487 × 18,519

Table 2. Standard metadata information for the raster datasets used in the study.

3.3 LSTM Model

3.3.1 Model Architecture: Recurrent Neural Networks (RNNs) Elman (1990) are a class of neural architectures designed for modeling sequential data by maintaining a hidden state that evolves over time, allowing the model to capture temporal dependencies within sequences. This makes RNNs particularly suitable for time series forecasting, natural language processing, and other tasks where the context of previous time steps influences current predictions.

However, because of their recurrent structure, traditional RNNs suffer from vanishing and exploding gradient problems, which occur when gradients shrink or grow exponentially through successive weight updates thereby impairing the model's ability to capture long-term dependencies in sequential data. To ad-

dress this limitation, an augmented version of the RNN known as the *Long Short-Term Memory* (LSTM) network Hochreiter and Schmidhuber (1997) was used in this study.

LSTM capture long-range dependencies in sequences by incorporating a memory cell and a set of gating mechanisms. These gates regulate the flow of information, enabling the network to retain or discard information over long periods.

The LSTM computations at each time step t are defined as follows:

$$f_t = \sigma(W_f[x_t, h_{t-1}] + b_f) \tag{1}$$

$$i_t = \sigma(W_i[x_t, h_{t-1}] + b_i) \tag{2}$$

$$\tilde{c}_t = \tanh(W_c[x_t, h_{t-1}] + b_c) \tag{3}$$

$$o_t = \sigma(W_o[x_t, h_{t-1}] + b_o) \tag{4}$$

$$c_t = f_t \odot c_{t-1} + i_t \odot \tilde{c}_t \tag{5}$$

$$h_t = o_t \odot \tanh(c_t) \tag{6}$$

where x_t = input vector at time step t
h_{t-1} = previous hidden state
c_{t-1} = previous cell state
f_t, i_t, o_t = forget, input, and output gates
$\tilde{c}_t$ = candidate cell state
$\sigma(\cdot)$ = sigmoid activation function
$\tanh(\cdot)$ = hyperbolic tangent activation function
$\odot$ = element-wise multiplication
W_*, b_* = weight matrices and bias vectors

By maintaining both a hidden state h_t and a cell state c_t, the LSTM module is able to carry information over longer sequences. This gating structure ensures that gradients remain stable during backpropagation.

3.3.2 Training and Validation: The LSTM framework was implemented using PyTorch with the hyperparameters listed in Table 3. The model was trained on an A100 GPU using CUDA, as the dataset was considerably large approximately 30 GB in memory and has over 29 million datapoints for the whole country. To facilitate efficient preprocessing prior to model training, libraries such as `cudf` from RAPIDS and `cupy` were utilized.

Hyperparameter	Value
Number of layers	3
Size of hidden layer	64
Dropout rate	0.30
Learning rate	0.001

Table 3. LSTM model hyperparameter settings.

The GAIA dataset from 2010 to 2020, concatenated with static features, served as the training data. A time series cross-validation approach was used to validate the model's performance on a per-year basis. Given the highly imbalanced nature of the dataset (i.e., non-urban pixels vastly outnumber urban pixels), techniques were explored to create a model that generalized better. First was undersampling of the majority class but this led to overprediction of urban areas during simulation. To better reflect the natural class imbalance observed in real-world scenarios, class weighting was ultimately used.

As discussed in Section 3.4.5, two main approaches can be used to convert potential probabilities into binary urban classifications: allocation using economic drivers and direct thresholding. Although population growth was also modeled and projected on a nationwide scale, it was difficult to establish a stable relationship between urban expansion and population trends. This difficulty was primarily due to the abrupt changes observed during the COVID-19 pandemic, particularly in 2021, which introduced a discontinuity in the urbanization trend Department of Trade and Industry (DTI) (2021). Consequently, the study restricted the training data to the 2010–2020 period and employed thresholding as the primary classification approach.

To calibrate the appropriate threshold, the RAPIDS cuML metrics' Python library Precision-Recall (P-R) curve was used during validation. For each year, the precision and recall outputted by the function were used to compute the F1 score across various thresholds. The threshold yielding the highest average F1 score was then selected as the calibrated threshold for subsequent testing and simulation.

3.4 CA Model

As outlined in Section 2.1, CA models comprise several core components: the transition probability surface, neighborhood effects, geographical constraints, and stochastic perturbations. These components are integrated as follows:

$$U^t_{\text{potential},ij} = U^t_{\text{transition},ij} \times U^t_{\Omega,ij} \times SP^t_{ij} \times C_{ij} \tag{7}$$

3.4.1 Transition probability: $U^t_{\text{transition},ij}$ denotes the suitability of pixel p_{ij} for urban transition, based on multiple spatial factors—commonly referred to as *transition rules*. Early CA-based urban models implemented these rules through explicit "if-then" logic, consistent with classical CA theory. Over time, these rules evolved into probabilistic formulations—termed suitability surfaces which integrate diverse spatial factors Li and Gong (2016); Santé et al. (2010). Such surfaces are often generated using logistic regression models, calibrated with explanatory variables like distance to transport infrastructure, water bodies, and urban centers Yang et al. (2020); Li and and (2004). The local literature Johnson et al. (2021), which serves as the main basis for this study, employs a similar logistic regression framework to derive a static transition probability surface, assumed static over time.

This study, however, tries to improve the simulation methodology by incorporating a machine learning model specifically LSTM networks, as elaborated in Section 3.3. The objective is to produce a dynamic transition probability matrix that evolves over time, thereby reflecting the changing likelihood of land undergoing urban transition. This is achieved by incorporating spatiotemporal features such that, given the simulation output at time t, a set of spatial urban features is computed and used as input for predicting urban transition at $t + 1$.

3.4.2 Neighborhood effects: $U^t_{\Omega,ij}$ represents the influence of neighborhood configurations technically referred to as spatial lag effects Feng et al. (2018). This component is typically computed using a predefined neighborhood structure, such as Moore's neighborhood, and its spatial extent. This study build the CA system as presented on the on the recent trend-adjusted neighborhood framework Li et al. (2020) which incorporates historical urbanization data. Here, more recently urbanized neighbors exert greater influence than those developed earlier.

$$W^t_{ij} = 1 - \frac{N^u_{ij}}{N}, \tag{8}$$

$$U^t_{\Omega,ij} = \frac{\sum_{m\times m} \text{Condition}(p_{ij} = \text{urban}) \times W^t_{ij}}{m \times m - 1} \tag{9}$$

where W^t_{ij} = temporal weighting factor for cell (i, j)

N_{ij}^{u} = number of years cell (i, j) has been urban
N = total simulation period
Condition() = returns 1 if neighbor cell is urban, 0 otherwise
m = neighborhood window size

3.4.3 Stochastic perturbations: SP_{ij}^{t} simulates the real-world randomness. There are two primary approaches used for calculating this factor, Monte Carlo-based methods Yeh and Li (2006), and the *disturbance function* White and Engelen (1993). This study adopts the latter due to its simplicity yet prevalence in studies of urban CA models:

$$SP_{ij}^{t} = 1 + (-\ln \lambda)^{\alpha} \tag{10}$$

where λ = random variate drawn from a uniform distribution $[0, 1]$
α = hyperparameter controlling perturbation intensity

The resulting distribution is highly skewed as most resulting values are near 1, with occasional larger deviations to ensure that the transition probabilities and neighborhood components remain as dominant components in the urban sprawl simulation.

3.4.4 Constraints: C_{ij} defines static factors that prohibit urban development. These include natural barriers such as bodies of water, steep slopes, and protected areas. In this study, the constraint factor is limited only to water and defined as:

$$C_{ij} = \begin{cases} 0, & \text{if cell (i,j) = water} \\ 1, & \text{otherwise} \end{cases} \tag{11}$$

3.4.5 Potential probability: $U_{\text{potential},ij}^{t}$ represents the combined suitability of pixel (i, j) for urban change after integrating transition rules, spatial influence, randomness, and physical constraints. This potential surface can be operationalized using two dominant transformation strategies:

- **Allocation-based approach**, which allocates a fixed number of urban transitions based on external indicators, most often projected population, to maintain target ratios between urban extent and used indicator Johnson et al. (2021).
- **Threshold-based approach**, which classifies pixels as urban if $U_{\text{potential},ij}^{t}$ exceeds a specified threshold, typically 0.5 Li et al. (2014).

3.4.6 Testing and Simulation: As mentioned in Section 3.3.2, a major discontinuity occurred in 2021 in the urbanization trend across the country. Due to this, the testing and simulation phase began with input data from 2021 to simulate urban maps from 2022 to 2030. During simulation, the output map for year t was used as input for year $t + 1$. For example, urban map of year 2021 was used to predict the urban map for 2022, which was then used to derive the map for year 2023, and so on. Since the available dataset only extended to 2024, model predictions were compared against actual data only for the years 2022 to 2024 using the two evaluation metrics commonly used in urban change literatures:

1. **Fuzzy Similarity Rating (FSR)** evaluates spatial neighborhood agreement rather than per-pixel exact matches. It calculates the maximum of a set of exponentiated predictions as shown in belowm where d is the Manhattan distance from a predicted pixel to the actual target pixel. This was applied to all newly predicted urban from 2022 to 2024, compared with the actual newly urbanized areas over the same period (aggregated into a single map).

$$\text{FSR}\ (\%) = \frac{\sum_{ij \in p_{\text{urban, pred}}} \max\left((1/2)^{0/2}, \ldots, (1/2)^{d/2}\right)}{\sum_{ij \in p_{\text{urban, actual}}} 1} \tag{12}$$

$$p_{ij} = \begin{cases} 1, & \text{if cell } (i, j) \text{ in the predicted map has the same land-use class within a neighborhood of radius } d \text{ in the actual map} \\ 0, & \text{otherwise} \end{cases} \tag{13}$$

2. **Figure of Merit (FOM)** measures the overlap between modeled and observed maps, focusing on changed pixels. It is widely used in land change studies as it offers a more robust performance evaluation:

$$\text{FOM}\ (\%) = \frac{\text{TP}}{\text{TP} + \text{FN} + \text{FP}} \tag{14}$$

where TP = correctly predicted urbanized pixels
FP = pixels incorrectly predicted
FN = actual urban pixels not predicted

4. Results and Discussion

4.1 Model Calibration

The hyperparameters for the CA model are summarized in Table 4. These values were selected after an extensive calibration process that balanced prediction quality and generalization.

Hyperparameter	Value
Stochastic α	1
Neighborhood Window	3
Trend Years	10
Calibrated Threshold	0.90

Table 4. Calibrated hyperparameter settings for the CA model.

4.2 Model Performance Metrics

The performance of the LSTM-based models based on FSR is shown in Table 5. The LSTM-CA model outperformed both the standalone LSTM and reference literature. Luzon and Visayas recorded notably high FSR scores for LSTM-CA at 48.15% and 47.91%, respectively, whereas Mindanao showed more moderate performance (18.53%). This suggests that while LSTM-CA effectively captures spatial patterns in denser urban regions, challenges remain in more dispersed areas.

Region	Model		
	LSTM-CA	LSTM	CA
Luzon	48.15	9.63	10.18
Visayas	47.91	12.39	5.63
Mindanao	18.53	19.50	11.78
Average	**38.20**	**13.84**	**9.20**

Table 5. Comparison of FSR scores across Philippine island groups for different urban growth models.

FOM values from 2022 to 2024 are presented in Table 6. The LSTM-CA model achieved the highest FOM scores for

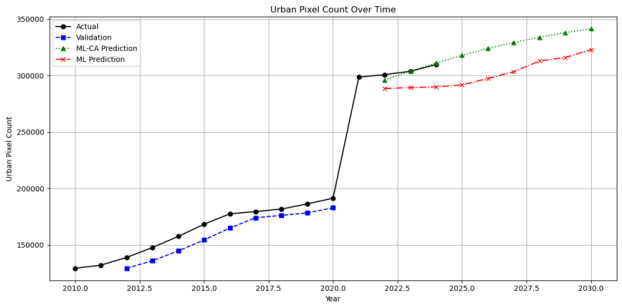

Figure 6. Validation and Testing Result for Luzon.

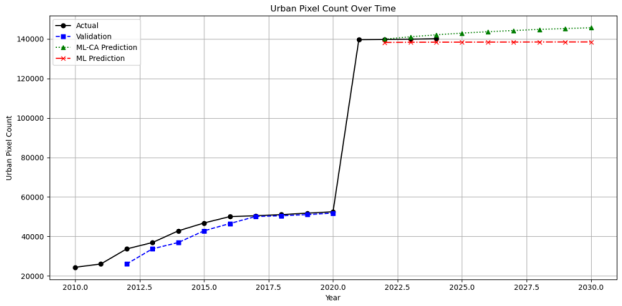

Figure 7. Validation and Testing Result for Visayas.

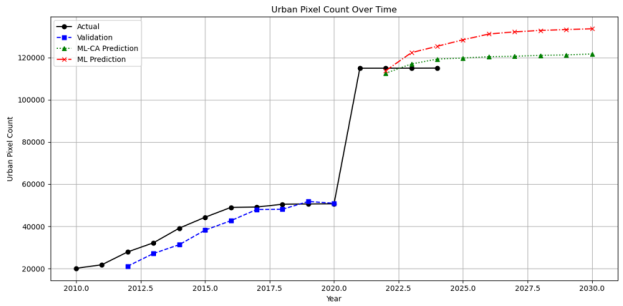

Figure 8. Validation and Testing Result for Mindanao.

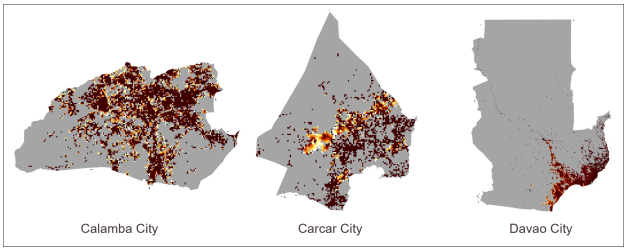

Figure 9. Projected top urban growth hotspots by 2030 for each major region of the Philippines: Calamba (Luzon), Carcar (Visayas), and Davao (Mindanao).

all years, with an average of 0.5537, reflecting its stronger alignment with observed newly urbanized areas. The standalone LSTM and CA models consistently underperformed, emphasizing the benefit of hybrid ML-CA model.

Year	Model		
	LSTM-CA	LSTM	CA
2022	0.5603	0.3594	0.3077
2023	0.5524	0.3529	0.2805
2024	0.5485	0.3480	0.2570
Average	**0.5537**	**0.3534**	**0.2817**

Table 6. FOM scores from 2022 to 2024 for each model.

Figures 6, 7, and 8 show yearly trends in urban pixel counts during both validation and simulation phases. In Luzon, the validation results closely follow the actual urban growth trend with minor underprediction, while the test results exhibit strong alignment with actual values. This indicates good generalization of the model in more urbanized areas.

In Visayas and Mindanao, validation results similarly match the actual trends starting 2017. However, in the testing and simulation period, the model tends to overpredict urban pixel counts. This discrepancy can be attributed to the stagnation observed in actual urbanization during this period likely influenced by post-pandemic slowdowns in construction and infrastructure development. Since the model is trained on pre-2020 trends, it continues to forecast growth that did not manifest in reality.

In addition to accuracy-based metrics, the computational efficiency of the models were also monitored. Results show that the hybrid LSTM-CA model is almost twice as slow as the standalone CA approach, largely due to the additional training requirements of the LSTM component. However, the runtime of LSTM-CA and standalone LSTM models is nearly the same, indicating that the integration of CA contributes only minimal computational overhead beyond what is already required for LSTM training.

4.3 Simulation of Urban Sprawl in the Philippines by 2030

Using the localized predictions, simulation maps were generated to identify the year in which each pixel transitioned to an urban state. These maps were then aggregated at the city level using the official Philippine boundary dataset Faeldon (2024). From this aggregation, various urbanization metrics were derived, including the cities that experienced the most significant increase in urban pixels.

Figure 9 presents examples of such trends, highlighting Calamba City, which showed an increase from 4,389 urban pixels in 2025 to 5,317 by 2030. Similarly, Carcar increased from 1,809 to 2,162 pixels, while Davao expanded from 1,651 to 2,161 pixels over the same period. Additional analyses from the simulated maps may include identifying cities with the highest percentage increase in urban area or those that did not experience any new urbanization.

It is important to note that the current simulation relies solely on a physical expansion model. Urban growth is modeled based on spatial trends, specifically how the GAIA dataset defines urbanity (i.e., built-up areas). Socioeconomic or policy-driven factors are not incorporated at this stage.

5. Conclusion and Recommendations

The combined LSTM-CA model demonstrated superior performance over the traditional Logistic Regression-CA model, underscoring the advantage of employing a dynamic suitability surface that evolves through time. This approach significantly enhanced the model's capability to simulate pixel-level urban transitions, capturing complex spatio-temporal patterns more realistically. Additionally, it outperformed the standalone LSTM by incorporating spatial perturbations and neighborhood-weighted factors, which contributed to a more context-aware representation of urban growth.

These results can be further utilized for broader spatial planning applications. For instance, the predicted urban expansion maps can be overlaid with agricultural land-use layers to quantify the extent and location of agricultural land conversion, helping assess risks to food security. Similarly, by integrating the simulated urban growth with road network data, urban connectivity can be evaluated through measures such as changes in travel time or accessibility indices, thereby identifying areas requiring transport infrastructure investment. Furthermore, the outputs can be linked with socio-economic datasets to estimate productivity impacts of urban expansion by analyzing how new urban areas coincide with economic zones or labor markets. In this way, the dynamic forecasts generated by the LSTM-CA framework can directly feed into scenario-based spatial planning, providing planners and policymakers with actionable insights for balancing development, mobility, and sustainability.

To improve the study further, one key direction is the refinement of metrics used to determine urban expansion rates. Currently, the model uses the increase in urban pixels as a proxy for expansion intensity, which may not fully capture underlying dynamics. A more robust approach would involve integrating population growth or economic indicators.

Enhancing the model's accuracy can also be achieved through comprehensive hyperparameter tuning of the LSTM component.

Finally, exploring alternative model architectures such as Attention-Based LSTM or Transformer models may further enhance the model's ability to capture more intricate spatial-temporal interactions in urban development patterns.

References

Cao, T.-T., Tang, K., Mohamed, A., Tan, T.-S., 2010. Parallel banding algorithm to compute exact distance transform with the gpu. *Proceedings of the 2010 ACM SIGGRAPH Symposium on Interactive 3D Graphics and Games*, I3D '10, Association for Computing Machinery, New York, NY, USA, 83–90.

Chaves, C., Eustaquio, J., Marcall, A., 2022. Modeling Settlements Development in the Philippines. *Transactions of the National Academy of Science and Technology*, 43.

Department of Trade and Industry (DTI), 2021. Construction industry contributes 16.6% to gdp amidst pandemic. Date of Release: 27 August 2021.

Elman, J. L., 1990. Finding structure in time. *Cognitive Science*, 14(2), 179-211.

Estoque, R. C., Murayama, Y., 2012. Examining the potential impact of land use/cover changes on the ecosystem services of Baguio city, the Philippines: A scenario-based analysis. *Applied Geography*, 35(1), 316-326.

Faeldon, J., 2024. Philippines psgc administrative boundaries shapefiles. github.com/altcoder/philippines-psgc-shapefiles. Accessed: 2024-12-01.

Feng, Y., Yang, Q., Hong, Z., and, L. C., 2018. Modelling coastal land use change by incorporating spatial autocorrelation into cellular automata models. *Geocarto International*, 33(5), 470–488.

Gong, P., Li, X., Wang, J., et al., 2020. Annual maps of global artificial impervious area (GAIA) between 1985 and 2018. *Remote Sensing of Environment*, 236, 111510. Data available at data-starcloud.pcl.ac.cn/iearthdata/13. Accessed: 2025-05-29.

Gómez, J. A., Patiño, J. E., Duque, J. C., Passos, S., 2020. Spatiotemporal Modeling of Urban Growth Using Machine Learning. *Remote Sensing*, 12(1).

Hochreiter, S., Schmidhuber, J., 1997. Long Short-Term Memory. *Neural Computation*, 9, 1735-1780.

Johnson, B. A., Estoque, R. C., Li, X., Kumar, P., Dasgupta, R., Avtar, R., Magcale-Macandog, D. B., 2021. High-resolution urban change modeling and flood exposure estimation at a national scale using open geospatial data: A case study of the Philippines. *Computers, Environment and Urban Systems*, 90, 101704.

Karra, K., Kontgis, C., Statman-Weil, Z., Mazzariello, J. C., Mathis, M., Brumby, S. P., 2021. Global land use / land cover with sentinel 2 and deep learning. *2021 IEEE International Geoscience and Remote Sensing Symposium IGARSS*, 4704–4707.

Kim, Y., Safikhani, A., Tepe, E., 2022. Machine learning application to spatio-temporal modeling of urban growth. *Computers, Environment and Urban Systems*, 94, 101801.

Li, X., and, A. G.-O. Y., 2004. Data mining of cellular automata's transition rules. *International Journal of Geographical Information Science*, 18(8), 723–744.

Li, X., Gong, P., 2016. Urban growth models: progress and perspective. *Science Bulletin*, 61(21), 1637–1650.

Li, X., Liu, X., and, L. Y., 2014. A systematic sensitivity analysis of constrained cellular automata model for urban growth simulation based on different transition rules. *International Journal of Geographical Information Science*, 28(7), 1317–1335.

Li, X., Zhou, Y., Chen, W., 2020. An improved urban cellular automata model by using the trend-adjusted neighborhood. *Ecological Processes*, 9(1), 28.

Meijer, J. R., Huijbregts, M. A. J., Schotten, K. C. G. J., Schipper, A. M., 2018. Global patterns of current and future road infrastructure. *Environmental Research Letters*, 13(6), 064006.

Philippine Statistics Authority (PSA), 2022. Urban population of the philippines (2020 census of population and housing). Accessed: 2024-12-01.

Reuter, H. I., Nelson, A., Jarvis, A., 2007. An evaluation of void filling interpolation methods for SRTM data. *International Journal of Geographic Information Science*, 21(9), 983–1008.

Rienow, A., Mustafà, A., Krelaus, L., Lindner, C., 2021. Modeling urban regions: comparing random forest and support vector machines for cellular automata. *Transactions in GIS*, 25, 1625-1645.

Rousseeuw, P. J., 1987. Silhouettes: A graphical aid to the interpretation and validation of cluster analysis. *Journal of Computational and Applied Mathematics*, 20, 53-65.

Roy, S., Jensen, E., Saah, A., Swetnam, T., 2025. samapriya/awesome-gee-community-datasets: Community catalog (version 3.5.0). Accessed: 2025-05-29.

Santé, I., García, A. M., Miranda, D., Crecente, R., 2010. Cellular automata models for the simulation of real-world urban processes: A review and analysis. *Landscape and Urban Planning*, 96(2), 108-122.

UN-Habitat, 2023. Un-habitat philippines country report 2023. Accessed: 2024-12-01.

White, R., Engelen, G., 1993. Cellular Automata and Fractal Urban Form: A Cellular Modelling Approach to the Evolution of Urban Land-Use Patterns. *Environment and Planning A: Economy and Space*, 25(8), 1175-1199.

Wu, F., Martin, D., 2002. Urban Expansion Simulation of Southeast England Using Population Surface Modelling and Cellular Automata. *Environment and Planning A: Economy and Space*, 34(10), 1855-1876.

Yang, J., Gong, J., Tang, W., Liu, C., 2020. Patch-based cellular automata model of urban growth simulation: Integrating feedback between quantitative composition and spatial configuration. *Computers, Environment and Urban Systems*, 79, 101402.

Yeh, A. G.-O., Li, X., 2006. Errors and uncertainties in urban cellular automata. *Computers, Environment and Urban Systems*, 30(1), 10-28.